

Article

The Determination of the Sensitivity of Refractive Index Sensors

Ilya M. Efimov * , Nikolay A. Vanyushkin and Ashot H. Gevorgyan 

Institute of High Technologies and Advanced Materials, Far Eastern Federal University, 10 Ajax Bay, Russky Island, 690922 Vladivostok, Russia; vanyushkin.na@dvgfu.ru (N.A.V.); gevorgyan.aa@dvgfu.ru (A.H.G.)

* Correspondence: efimov.im@dvgfu.ru; Tel.: +7-914-666-82-00

Abstract: A new approach to determining the sensitivity of refractive index sensors is proposed. It has been shown that relative and absolute sensitivity show different results, and also, for the first time, it is demonstrated that relative sensitivity has advantages over absolute sensitivity. In addition, the influence of the relative width of the photonic band gap and the difference in the refractive indices of the layers on the sensitivity are examined and the corresponding dependences of these parameters are obtained. We propose these parameters as a convenient tool for optimizing the sensitivity of sensors based on defective photonic crystals. Finally, results are obtained regarding the behavior of the defect mode at the center of the photonic band gap of one-dimensional photonic crystals.

Keywords: sensitivity; refractive index sensors; photonic crystals

1. Introduction

With the advent of optical methods of substance research, humanity has entered a new era of optics and photonics, and optical sensors are under active development in science and industry. Optical sensors are instruments that use the optical properties of an object to measure various parameters. In various fields such as manufacturing, robotics, medicine, and even home appliances, optical sensors are already widely used. They may be active, in which case they generate their own light and measure their reflection, transmission, or absorption, or passive, in which case they detect only light from other sources [1–4]. Research in the field of optical sensors is of great importance because the use of optical sensors has a number of advantages over other methods of analyzing matter; in particular, they are a non-contact method and have high accuracy [5]. Of course, there are also drawbacks, including certain difficulties associated with the unambiguous interpretation of signals [5].

This is the reason for a great number of papers written in the field of optical sensors, in particular refractive index sensors [6–37], aiming to find solutions to the following issues: extending their operating range, improving stability and reliability, decreasing costs, and increasing the availability, resolution, and sensitivity of the sensors. In particular, works [11–37] study the dependence of the sensitivity of refractive index sensors on various parameters. Works [11–13] use different operating ranges to increase sensitivity and also carry out comparative analyses of identical structures in different ranges. Works [14–26] focus on the effect of different types of sensor structures on the sensitivity of optical devices. The sensitivity of optical devices depends on the properties of the object under investigation; thus, the sensitivity of the same sensor can be different when used for different objects. The influence of such parameters is considered in works [11,13,24–33]. Works [16,22,31–37] investigate the influence of incidence angle on sensitivity.

One can see that sensitivity is widely used in the comparative analysis given in these articles and is often presented as a final parameter in order to demonstrate the advantage of a new sensor with respect to sensors with lower sensitivity. The present paper introduces an alternative approach to determining sensitivity, taking into account the resolution of



Citation: Efimov, I.M.; Vanyushkin, N.A.; Gevorgyan, A.H. The Determination of the Sensitivity of Refractive Index Sensors. *Photonics* **2024**, *11*, 56. <https://doi.org/10.3390/photonics11010056>

Received: 16 November 2023

Revised: 20 December 2023

Accepted: 2 January 2024

Published: 4 January 2024



Copyright: © 2024 by the authors. Licensee MDPI, Basel, Switzerland. This article is an open access article distributed under the terms and conditions of the Creative Commons Attribution (CC BY) license (<https://creativecommons.org/licenses/by/4.0/>).

the sensor. The question of which parameters should be considered when optimizing sensitivity is also considered.

Sensitivity is used to characterize refractive index sensors in most works [6–37]. In our work, we will consider this parameter using a photonic sensor based on a 1D photonic crystal (PC) with a defect layer (DL) as an example. A PC [38–41] is a periodic structure of layers with different refractive indices. PCs have a unique property of having a certain range of frequencies, called a photonic bandgap (PBG), in which electromagnetic waves cannot propagate through the PC. If a DL is added to the periodic structure of the PC, the periodicity of the structure is violated, which leads to changes in the transmission and reflection spectra in the entire region. In particular, this is represented by the appearance of a narrow band within the PBG, called the defect mode (DM), which is highly sensitive to changes in the DL parameters and is used for sensing.

2. Theory

2.1. Model of the Refractive Index Sensor

Our model of a refractive index sensor consists of two ideal PCs with a DL between them. Each PC consists of N periodic unit cells, where each cell is a pair of layers with thickness $h_{1,2}$ and refractive index $n_{1,2}$.

Between the two PCs, a DL is located, and in our model, it is the refractive index of the DL that changes under external influence. The DL in the PC violates its periodic structure and changes the light transmission properties, and DMs appear. The position of the DM depends on the many physical properties of the DL, such as the refractive index and the thickness of the DL.

In our case, the ideal PCs are mirrored with respect to the DL, with the DL bordering the layer that has the higher refractive index. It was shown in [25,26] that this configuration provides the highest sensitivity of the sensor and field localization in the DL.

Figure 1 shows a schematic diagram of our structure.

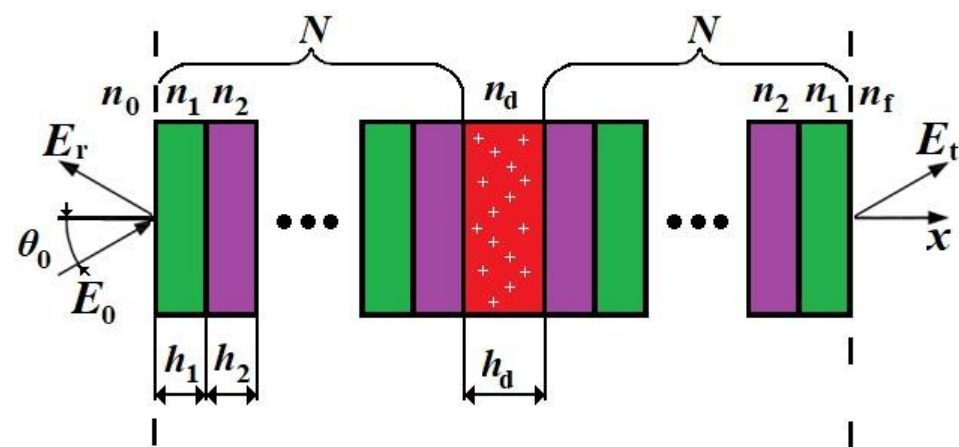


Figure 1. Schematic diagram of the structure under investigation. N is the number of unit cells, θ_0 is the angle of incidence, E_r is the reflected wave, E_0 is the incident wave, E_t is the transmitted wave, and n_0 and n_f are refractive indices of the structure surroundings.

In this work, we used the transfer matrix method [42–45] to calculate the transmission and reflection spectra of the investigated structure. The transfer matrix for the j -th layer in the structure can be written as:

$$M_j = \begin{pmatrix} \cos k_j h_j & \frac{-i}{p_j} \sin k_j h_j \\ -ip_j \sin k_j h_j & \cos k_j h_j \end{pmatrix}, \quad (1)$$

where $k_j = \frac{2\pi}{\lambda} n_j \cos \theta_j$, θ_j is the angle of refractive in the j -th layer, which is determined from Snell's law as: $\theta_j = \cos^{-1} \sqrt{1 - \frac{n_0^2 \sin^2 \theta_0}{n_j^2}}$, $p_j = n_j \cos \theta_j$, n_0 is the refractive index of the external medium from where the wave is incident, and θ_0 is angle of incidence.

Then, the matrix M of a unit cell in the periodic part of the structure is obtained by successive multiplication of the matrices M_j ($j = 1, 2$) of the layers contained in the cell, and finally, the transfer matrix of the whole structure has the form:

$$m = (M_1 M_2)^N M_d (M_2 M_1)^N = \begin{pmatrix} m_{11} & m_{12} \\ m_{21} & m_{22} \end{pmatrix}, \quad (2)$$

where M_d is the transfer matrix of the DL.

The transmission coefficient has the following form:

$$t = \frac{2p_0}{(m_{11} + p_f m_{12})p_0 + (m_{21} + p_f m_{22})}, \quad (3)$$

and the energy transmittance has the form:

$$T = \frac{p_f}{p_0} |t|^2, \quad (4)$$

where the indices 0,f denote the corresponding parameters of the medium bordering the PC on the left and right, respectively.

2.2. Principal Operating Mechanism of the Sensor

The refractive index of the DL can be obtained from the model as follows. To complete this, let us look at the transmission spectra in Figure 2. The black arrow shows the defect mode shift by $d\lambda$ when the refractive index of the defect layer changes, while all other parameters are the same. This shift can be used to determine the change in the DL refractive index n_d . This is the basis of sensor operation. In particular, the main idea of sensitivity is to show how much the DM shifts at the same change of the refractive index.

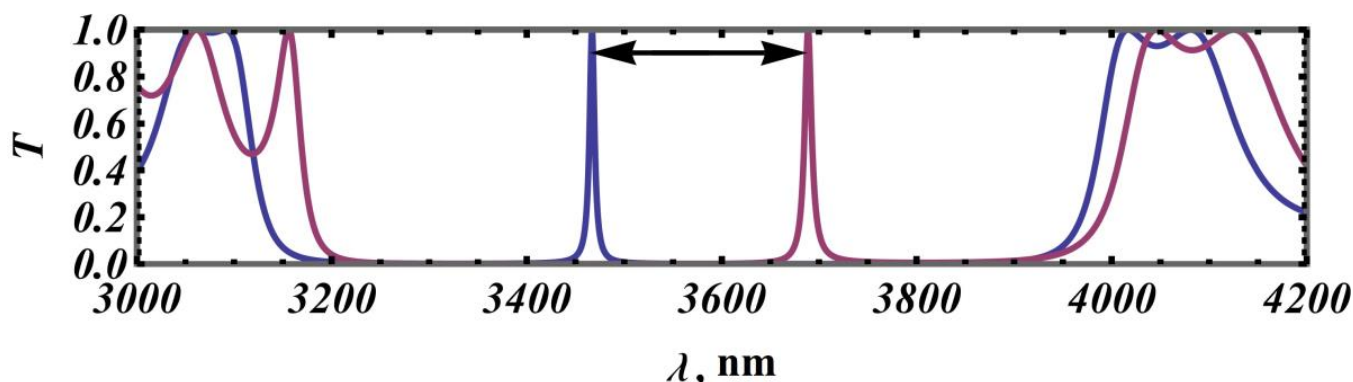


Figure 2. Transmission spectra of the defective PC with two different values of n_d . The blue line is the spectrum for a pure defective layer, and the red line is for a defective layer with inclusions.

2.3. Absolute and Relative Sensitivities

As we have already mentioned, in most of the works [9–37] devoted to refractive index sensors, a parameter such as sensitivity is used to characterize them. In the present work, we will call such sensitivity the absolute sensitivity, and in this case, the absolute sensitivity will be defined as follows:

$$S_a = \frac{d\lambda}{dn}, \quad (5)$$

Here, dn is the change in the refractive index of the medium and $d\lambda$ is the spectrum or mode shift that occurs due to the change in the refractive index.

The absolute sensitivity S_a of refractive index sensors is an important characteristic that determines how well the sensor can detect a change in the refractive index of interest. However, absolute sensitivity does not take into account the operating wavelength range and has a length dimension such as nm.

There is, however, a less commonly used analogue of absolute sensitivity. This is relative (or dimensionless) sensitivity S_r (see, in particular, [11,12,33]):

$$S_r = \frac{1}{\lambda_0} \frac{d\lambda}{dn}, \quad (6)$$

where λ_0 is the working wavelength.

The relative sensitivity S_r , as well as the absolute sensitivity S_a , represents the shift in the DM position with the change in the refractive index of the DL. In addition, the relative sensitivity takes into account the working range of the wavelengths and is a dimensionless quantity.

For the frequency ν range, the same rules apply:

$$S_a = \frac{d\nu}{dn}, \quad S_r = \frac{1}{\nu_0} \frac{d\nu}{dn}, \quad (7)$$

From the works [11–37], it can be seen that the relative and absolute sensitivities do not agree with each other. In some cases, when comparing two sensors, a higher absolute sensitivity can correspond to a lower relative sensitivity and vice versa. In particular, Table 1 shows the comparative characteristics of the works [11–16].

Table 1. Comparative table of sensitivity at different wavelengths [11–16].

$S_a, \frac{\text{nm}}{\text{RIU}}$	λ_0, nm	S_r, RIU^{-1}	Article
1020	5293	0.1927	[11]
80	5295	0.0151	
347	1004	0.3456	
710	2026	0.3504	
260	1560	0.1667	[14]
197	1600	0.1231	
198	1620	0.1222	
173	1640	0.1055	
80	1800	0.0444	
5018	7299	0.6875	[15]
5092	7299	0.6977	
5031	7293	0.6899	
5013	7335	0.6834	
500	523	0.9560	[27]
496	533	0.9316	
490	541	0.9058	
487	547	0.8897	
475	557	0.8520	
454	577	0.7875	
405	611	0.6639	
145	764	0.1891	[28]
144	766	0.1881	
144	769	0.1879	
144	773	0.1863	
1300	1530	0.8497	[29]
515	1550	0.3322	

When looking at Table 1, it can be seen that within a single article, there is usually an agreement between the absolute and relative sensitivity, which is explained by the fact that within a single article, the authors try to stay within approximately the same wavelength range, but when considering different operating wavelengths, the situation changes. Thus, in most papers [9–37], it can be seen that the sensitivities of different structures at different operating wavelengths are compared with those from other articles. According to these comparative characteristics, conclusions are drawn about the performance of the structures, which are not always correct.

There is also another factor that should be taken into account, which is not present in the use of absolute sensitivity. We can conclude that in practice, not every shift $d\lambda$ and therefore not every change dn in the refractive index can be detected when solving the inverse problem of finding the unknown refractive index from a measured spectrum. We need to consider the resolving power of the optical instrument to determine the minimum detectable $d\lambda$ shift.

2.4. Optical Sensor Resolution

The resolution R of an optical sensor determines its ability to discriminate between small changes in the optical signal. Let us look at the resolving power of an optical spectrometer. The resolving power of a spectrometer determines its ability to separate closely spaced spectral lines. In other words, to distinguish details in the spectrum with high accuracy. For example, we have two peak wavelengths λ and $\lambda + d\lambda$, and they can be separated (or resolved) with a resolution of at least $R = \lambda/d\lambda$; otherwise, they merge [46–50].

The resolution is a dimensionless quantity [46–50] and in this paper, we will consider the following situation. Consider two working wavelengths of 1000 and 2000 nm. Let the same resolving power for the two wavelengths be given and let be $R = 1000$. This means that it is possible to resolve peaks $d\lambda = 1$ and 2 nm, correspondingly, and distinguish peaks with the same wavelength difference $d\lambda$ at different working wavelengths λ_0 .

3. Results and Discussion

3.1. Comparing Absolute to Relative Sensitivity

The main idea of this work is to show that the absolute sensitivity S_a is not a reliable parameter when evaluating sensor performance. This sensitivity depends proportionally on the operating wavelength and does not correctly reflect the sensor parameters.

To illustrate this fact, let us start with a numerical experiment. Let us consider the following 1D PC shown in Figure 1. The parameters of the model are as follows: $n_1 = 1.5$, $n_2 = 2.0$, $n_0 = n_f = 1$, $N = 10$, $\theta_0 = 0$, h_1 and h_2 take the values $h_1 = h_2 = 500$ k nm, and $h_d = 1050$ k nm, where k is the proportionality factor of the structure. It should be noted that the dispersion of refractive indices is not considered in this work because it affects sensitivity and complicates the analysis of the results. Since the working wavelengths of the spectra considered are different, dispersion can make a significant difference in the PC refractive indices' values and thus the sensitivity of such a sensor, so this factor has been excluded for the clarity of the results. Otherwise, for arbitrary realistic refractive indices for PC, the conclusions of the model are valid. With these parameters, the following spectra can be obtained, as shown in the series of plots in Figure 3.

Such a large difference in refractive indices was chosen to clearly illustrate the DM shift. In the above series of spectra, the first PBG is shown whose center wavelength λ_B can be obtained from the Bragg condition:

$$\lambda_B = 2\Lambda n_m, \quad (8)$$

where $\Lambda = h_1 + h_2$ is the unit cell period of the PC and $n_m = \frac{n_1 h_1 + n_2 h_2}{h_1 + h_2}$ is the average refractive index of the unit cell.

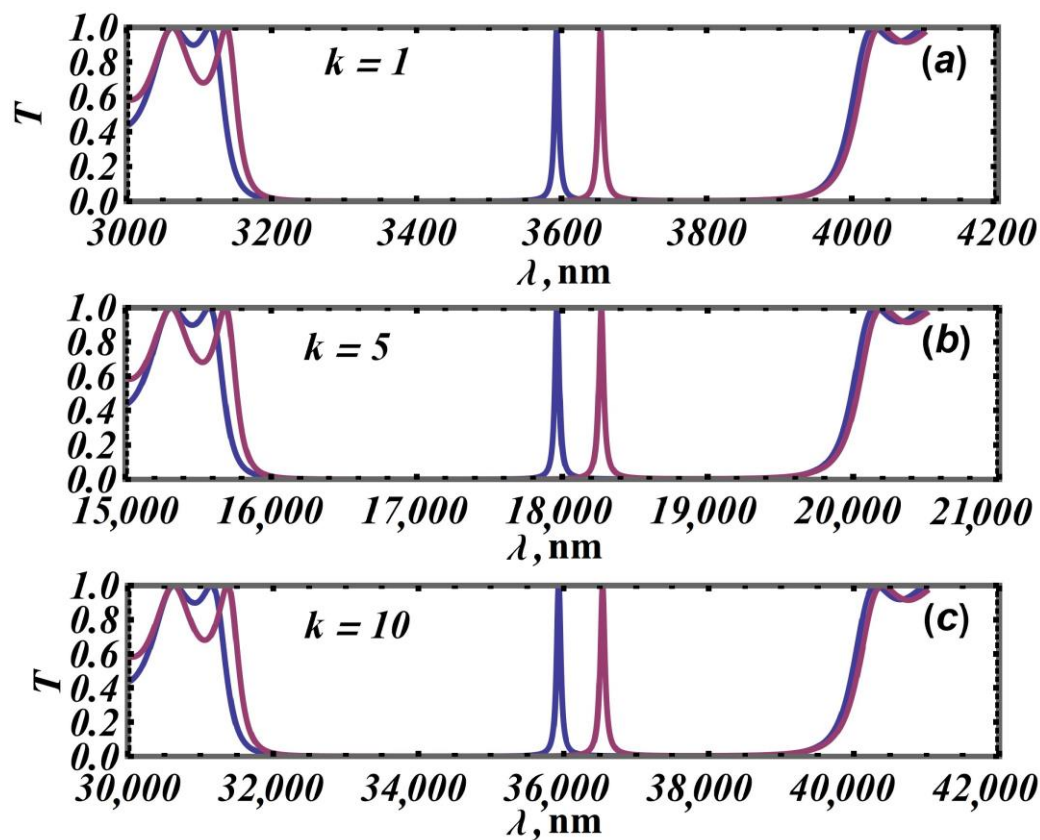


Figure 3. Transmission spectra at $n_d = 1.75$ and 1.90 (blue and red lines). The structure parameters are $n_1 = 1.5$, $n_2 = 2.0$, $N = 10$, $h_1 = h_2 = 500 \text{ } k \text{ nm}$, and $h_d = 1050 \text{ } k \text{ nm}$, (a) $k = 1$, (b) $k = 5$, (c) $k = 10$.

From the series of spectra in Figure 3 and Formula (8), it can be seen that the position of the first PBG is proportional to k . Also, it can be seen that the PBG widens; so, for $k = 1$, the width of the PBG is about 800 nm, and for $k = 10$, it is already 8000 nm. The shift in the DM also increases with increasing k for the same change in the refractive index of the DL. This directly affects the sensitivity S_a . Let us take a closer look at this influence in Table 2.

Table 2. Comparative values of different structures.

k	λ_B, nm	$S_a, \frac{\text{nm}}{\text{RIU}}$	S_r, RIU^{-1}
1	3500	440.33	
2	7000	880.65	
3	10,500	1320.98	
4	14,000	1761.30	0.1258074
5	17,500	2201.63	
10	35,000	4403.26	

It can be seen that the sensitivity S_a increases proportionally as k increases, and this is logical because as k increases, the shift in DM $d\lambda$ increases (the same change in the refractive index of the DL), while the relative sensitivity remains constant. According to the results of such a numerical experiment, it can be said that the two sensitivities produce different results. This can be seen when different operating ranges are considered in the same paper and their sensitivities are compared, or when different papers consider different operating ranges and compare their sensitivities. Furthermore, the definition of absolute sensitivity does not take into account the effect of the resolving power of the sensor. For this purpose, let us now consider the resolving power of the device.

As mentioned in Section 2.4, the higher the resolving power, the easier it is to determine the shift of the DM peak. Let us now consider a sensor with resolving power of $R = 1000$.

With this resolution it will be possible to distinguish a DM peak shift of 3.5 nm at a wavelength of 3500 nm and a DM peak shift of 7.0 nm at a wavelength of 7000 nm. Taking this into account, let us try to determine the minimum detectable change in the refractive index of the DL at constant resolving power; a comparison is given in Table 3.

Table 3. Comparative values of different structures at $R = 1000$.

k	$S_a, \frac{\text{nm}}{\text{RIU}}$	$S_a, \frac{\text{THz}}{\text{RIU}}$	S_r, RIU^{-1}	Min $\Delta\lambda, \text{nm}$	Δn_d
1	440.33	680.83		3.5	
2	880.65	340.42		7.0	
5	2201.63	136.17	0.1258074	17.5	0.002
10	4403.26	68.08		35.0	

As can be seen at a constant resolving power, structures with a different absolute sensitivity and the same relative sensitivity have the same ability to detect the change in the refractive index of the DL. We note another advantage of relative sensitivity, which is that the numerical relative sensitivity does not differ when the frequency or wavelength spectrum is considered. This result allows us to state that the relative sensitivity is a correct reflection of the structural properties, whereas the absolute sensitivity can be misleading.

3.2. Convenient Parameters for Optimizing the Sensitivity of a Sensor Based on 1D PCs with Defects

In this paper, it is also proposed to consider the influence of the relative and absolute PBG width on sensitivity ($\Delta\lambda/\lambda_B$ and $\Delta\lambda$). These parameters are affected by the large number of parameters of the structure. In particular, the PBG width can be varied by changing the layer thicknesses ratio h_1/h_2 with constant $n_1 = 1.5$ and $n_2 = 2.0$ and constant unit cell period $\Lambda = 1000$ nm. When this is carried out, the mean refractive index n_m of the unit cell changes and the width of the PBG changes correspondingly. The relative width of the PBG differs from the absolute one in that it is divided by the wavelength λ_B of the PBG center (see [44]). Figure 4 shows the dependence of the absolute sensitivity on the width of the PBG and that of the relative sensitivity on the relative width of the PBG for different numbers of unit cells N .

In the series in Figure 4, the green arrow shows the direction of increase in h_1 at the constant period of the unit cell of the PC. It can be seen that as the ratio h_1 to h_2 increases, the sensitivity increases and then starts to decrease. The dependence of the width of the PBG on the ratio h_1 to h_2 is considered in more detail in [51]. The red line marks the maximum PBG width, which corresponds to the quarter-wave stack $n_1 h_1 = n_2 h_2 = \lambda_B/4$. After the maximum point of the PBG width, a decrease in this width can be observed when the ratio h_1/h_2 is further increased. At the same time, the sensitivity decreases. It can also be observed in the series in Figure 4 that for the first and second ratio h_1/h_2 , the sensitivity values are different. However, one can see that these two sensitivities approach the same value as the number of periods increases. It can be assumed that in the case of an infinite PC with a defect, the two parts of the curve merge completely and the two sensitivities become equal.

It is important to note that the sensitivity values presented in the series in Figure 4 were obtained for the first DM mode; it can be shown that for other DMs, the general dependencies were preserved but shifted up. By changing the structural parameters for the series in Figure 4, the position of the center of the PBG λ_B was changed. Therefore, the thickness of the DL h_d was adjusted according to the center of the PBG so that the position of the DM λ_{DM} remained at the center of the PBG.

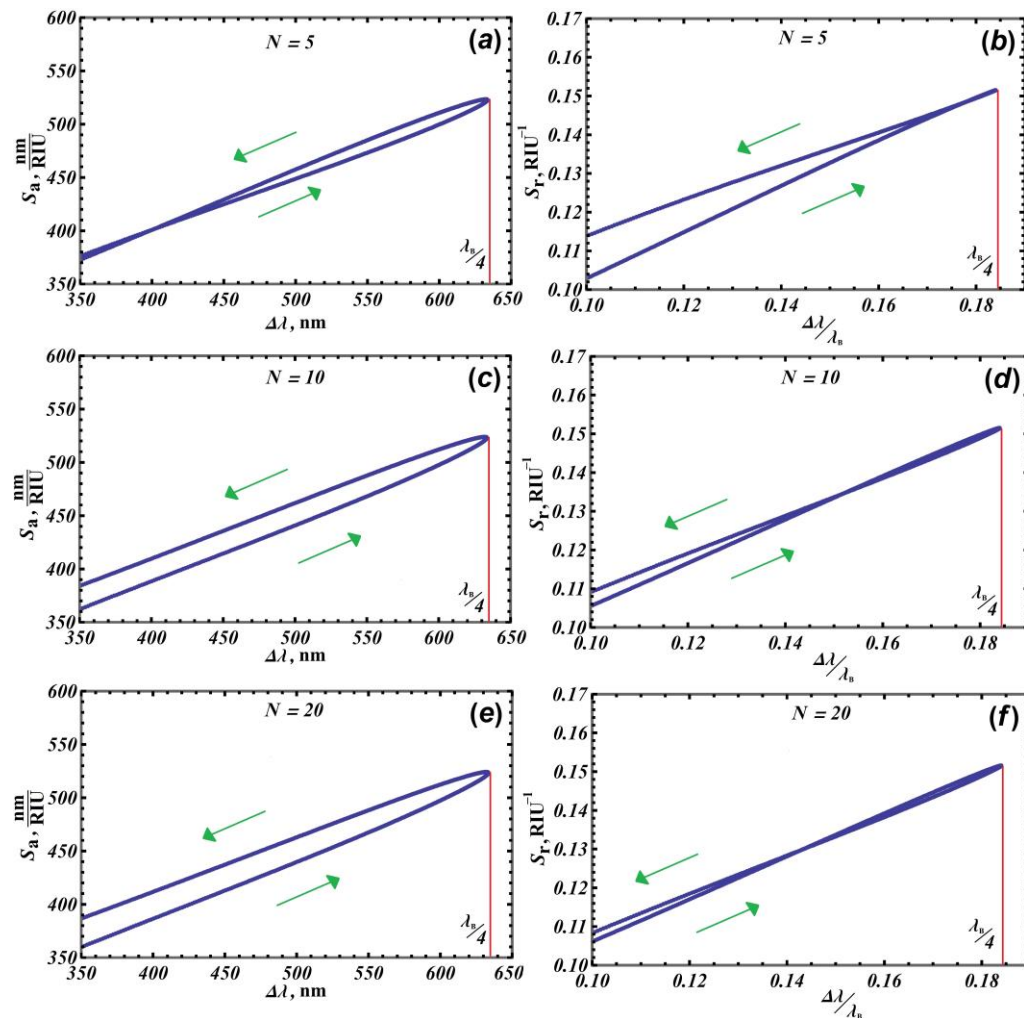


Figure 4. Dependence of absolute sensitivity on the width of the PBG (**a,c,e**) and that of the relative sensitivity on the relative width of the PBG (**b,d,f**). Here, $d\lambda$ is varied by changing h_1 . The green arrows indicate the increase in h_1 over a constant period. The red line marks the fulfillment of the quarter-wave stack. λ_B is the wavelength of the PBG center. The other parameters are the same as in Figure 3a.

In this paper, we argue that the width of the PBG, in particular the relative width of the PBG, is a convenient parameter for optimizing sensors based on 1D defect PCs. One of the main conclusions of this work is the following: for the relative sensitivity, we can unambiguously state that the maximum sensitivity is reached at the maximum PBG width. In particular, using this conclusion, it can be argued that to optimize a sensor based on a defective PC, the maximum of the relative width of the PBG should be aimed for. Thus, for the first PBG, it is necessary to use the quarter-wave stack.

Next, we will consider the dependence of sensitivity on the difference between the refractive indices $\Delta n = |n_1 - n_2|$, i.e., optical contrast, with a fixed mean refractive index.

Figure 5 shows the dependence of the relative PBG width on the refractive index difference (a) and the dependence of the relative sensitivity on the refractive index difference (b) under the following conditions: $n_m = \text{const}$ and $h_1 n_1 = h_2 n_2$.

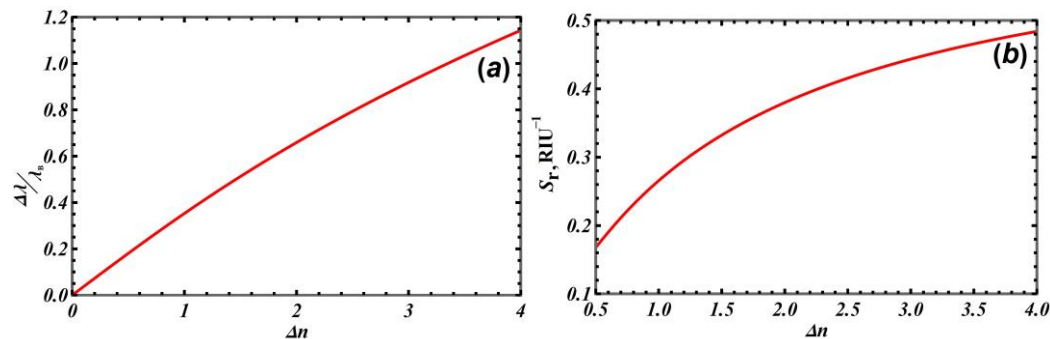


Figure 5. Dependence of the relative width of the PBG (a) and relative sensitivity (b) on the refractive index difference. The parameters are as follows: $n_m = 1.75$ and $h_1n_1 = h_2n_2 = \lambda_B/4$. The other parameters are the same as in Figure 3a.

Figure 5a shows that by increasing the refractive index difference of the unit cell layers, the relative bandwidth becomes larger, thus increasing the relative sensitivity. However, several interesting features should be noted. The dependence of the PBG width on Δn is not a linear function, but it is close to linear for sufficiently small values of Δn . In Figure 5b, we can see that the dependence of the relative sensitivity is correlated with the increase in the PBG width, but the width increases almost linearly, while the growth of the relative sensitivity slows down significantly and tends to a constant value (this is shown by our calculations).

When calculating the width of the PBG, the thickness of the DL is not taken into account as the calculation is for an infinite PC. However, to calculate the sensitivity, we need a certain thickness for the DL. The thickness of the DL was determined in the same way as in the series in Figure 4, i.e., the search is for such a thickness for the DL that the DM will be in the center of the PBG. In the case of the series in Figure 4, the values of the DL thickness were close to each other but still different.

When the thickness of the DL was calculated for Figure 5b, it was found that the thickness of the DL remained constant, i.e., the position of the DM depends only indirectly on h_1, n_1, h_2, n_2 the position of the DM depends primarily on the cell period Λ , the mean refractive index n_m , the parameters of the DL itself, the thickness h_d , and the refractive index of the DL n_d .

Figure 6 shows the evolution of the difference between the DM position and PBG center, with the change in the DL thickness h_d and the optical contrast Δn .

The position of the DM depends primarily on the cell period Λ , the mean refractive index n_m , the parameters of the DL itself, the thickness h_d , and the refractive index of the DL n_d . Thus, in Figure 6, it can be observed that the position of the DM does not shift when the refractive index difference Δn changes, as can be seen by the dark blue line in the center. This means that for the DM to be in the center of the PBG, the thickness of the DL h_d must take on a certain constant value, even when Δn changes.

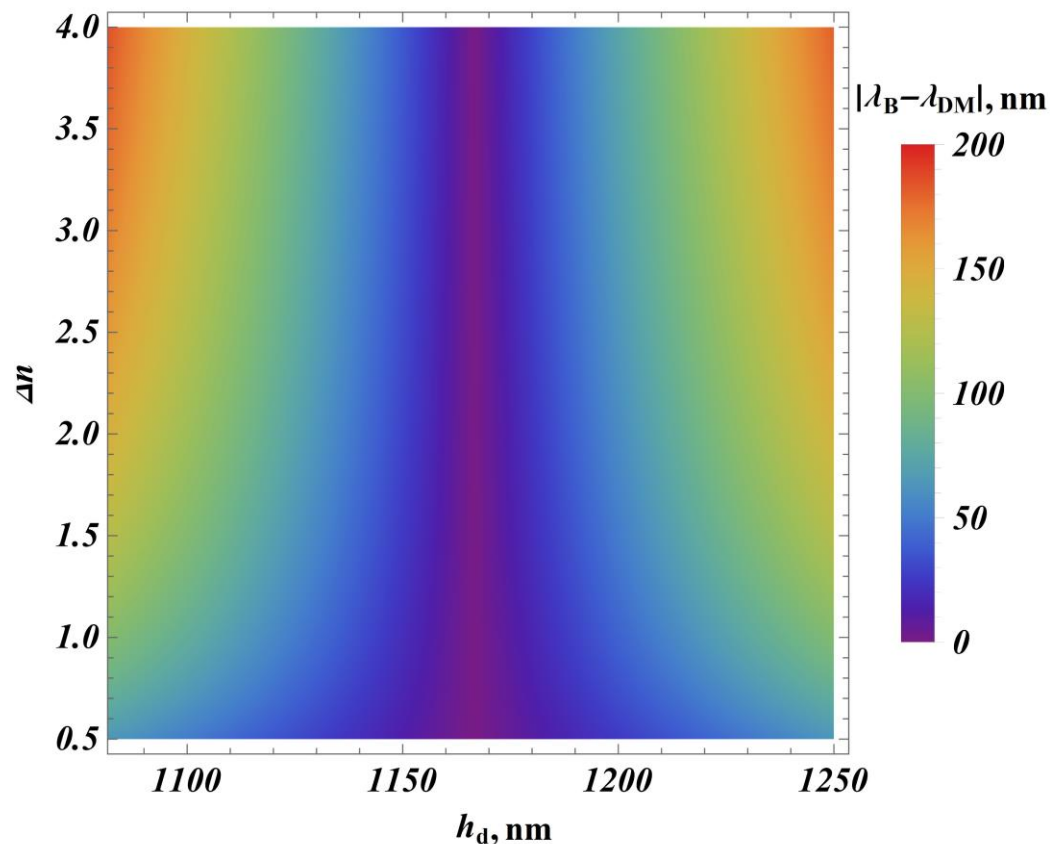


Figure 6. Dependence of the difference in the DM position λ_{DM} and the PBG center λ_B on the DL thickness h_d and the refractive index difference Δn . The parameters are the same as in Figure 5b.

4. Conclusions

In conclusion, we considered two types of sensitivity: relative and absolute. For the same structures, these two types of sensitivity were found to give different results. It was determined which parameters, such as operating wavelength and resolution, are also necessary for a correct evaluation; as a consequence, it has been shown that it is not correct to use absolute sensitivity in comparative evaluations of refractive index sensors. On the other hand, relative sensitivity has a number of advantages over its counterpart, and it has also been shown that it is relative sensitivity that is worth using in the comparative characterization of different structures at different operating wavelengths.

The effect of the width of the PBG on relative sensitivity has been shown. The maximum relative sensitivity was found to be at the maximum of the relative width of the PBG, i.e., at the quarter-wave stack. The dependence of the sensitivity on the refractive index difference was also studied. In this case, an increase in sensitivity is observed as the width of the PBG increases. However, the width increases almost linearly, whereas the increase in relative sensitivity slows down significantly and tends to a constant value.

In addition to the parameters of the DL itself, such as the thickness h_d and the refractive index of the DL n_d , the position of the DM in the center of the PBG was found to depend directly on the mean refractive index n_m and the cell period Λ .

Author Contributions: Conceptualization I.M.E., N.A.V. and A.H.G.; formal analysis N.A.V.; software I.M.E.; writing—original draft preparation I.M.E.; writing—review and editing I.M.E., N.A.V. and A.H.G.; project administration A.H.G. All authors have read and agreed to the published version of the manuscript.

Funding: This work was supported by the Foundation for the Advancement of Theoretical Physics and Mathematics “BASIS” (grant No. 21-1-1-6-1).

Institutional Review Board Statement: Not applicable.

Informed Consent Statement: Not applicable.

Data Availability Statement: Data are contained within the article.

Conflicts of Interest: The authors declare no conflicts of interest.

References

1. Santos, J.L.; Faramarz, F. *Handbook of Optical Sensors*; CRC Press: Boca Raton, FL, USA, 2014.
2. Ferreira, M.F.; Castro-Camus, E.; Ottaway, D.J.; López-Higuera, J.M.; Feng, X.; Jin, W.; Jeong, Y.; Picqué, N.; Tong, L.; Reinhard, B.M.; et al. Roadmap on optical sensors. *J. Opt.* **2017**, *19*, 083001. [[CrossRef](#)] [[PubMed](#)]
3. Tong, L. Micro/nanofibre optical sensors: Challenges and prospects. *Sensors* **2018**, *18*, 903. [[CrossRef](#)] [[PubMed](#)]
4. Kersey, A.D. A review of recent developments in fiber optic sensor technology. *Opt. Fiber Technol.* **1996**, *2*, 291–317. [[CrossRef](#)]
5. Grattan, K.T.; Sun, T. Fiber optic sensor technology: An overview. *Sens. Actuators A Phys.* **2000**, *82*, 40–61. [[CrossRef](#)]
6. Ma, S.; Xu, Y.; Pang, Y.; Zhao, X.; Li, Y.; Qin, Z.; Liu, Z.; Lu, P.; Bao, X. Optical Fiber Sensors for High-Temperature Monitoring: A Review. *Sensors* **2022**, *22*, 5722. [[CrossRef](#)] [[PubMed](#)]
7. Wang, Z.; Wang, G.; Kumar, S.; Marques, C.; Min, R.; Li, X. Recent advancements in resonant fiber optic gyro—A review. *IEEE Sens. J.* **2022**, *22*, 3195502. [[CrossRef](#)]
8. Chai, H.; Zheng, Z.; Liu, K.; Xu, J.; Wu, K.; Luo, Y.; Liao, H.; Debliquy, M.; Zhang, C. Stability of metal oxide semiconductor gas sensors: A review. *IEEE Sens. J.* **2022**, *22*, 5470–5481. [[CrossRef](#)]
9. Li, J.; Huang, X.; Tu, L.; Zhang, T.; Wang, L. A review of building detection from very high resolution optical remote sensing images. *GISci. Remote Sens.* **2022**, *59*, 1199–1225. [[CrossRef](#)]
10. Jayawickrema, U.M.N.; Herath, H.M.; Hettiarachchi, N.K.; Sooriyaarachchi, H.P.; Epaarachchi, J.A. Fibre-optic sensor and deep learning-based structural health monitoring systems for civil structures: A review. *Measurement* **2022**, *199*, 111543. [[CrossRef](#)]
11. Efimov, I.M.; Vanyushkin, N.A.; Gevorgyan, A.H.; Golik, S.S. Optical biosensor based on a photonic crystal with a defective layer designed to determine the concentration of SARS-CoV-2 in water. *Phys. Scr.* **2022**, *97*, 055506. [[CrossRef](#)]
12. Luan, E.; Shoman, H.; Ratner, D.M.; Cheung, K.C.; Chrostowski, L. Silicon Photonic Biosensors Using Label-Free Detection. *Sensors* **2018**, *18*, 3519. [[CrossRef](#)] [[PubMed](#)]
13. Dutta, H.S.; Goyal, A.K.; Srivastava, V.; Pal, S. Coupling light in photonic crystal waveguides: A review. *Photonics Nanostruct. Fundam. Appl.* **2016**, *20*, 41–58. [[CrossRef](#)]
14. Dutta, H.S.; Suchandan, P. Design of a highly sensitive photonic crystal waveguide platform for refractive index based biosensing. *Opt. Quantum Electron.* **2013**, *45*, 907–917. [[CrossRef](#)]
15. Ahmed, A.M.; Ahmed, M. Ultra-high sensitive 1D porous silicon photonic crystal sensor based on the coupling of Tamm/Fano resonances in the mid-infrared region. *Sci. Rep.* **2019**, *9*, 6973. [[CrossRef](#)] [[PubMed](#)]
16. Abdol, S.O.; Babak, A. Novel biosensors based on Weyl semimetals. *Phys. Scr.* **2022**, *97*, 125502. [[CrossRef](#)]
17. El Beheiry, M.; Liu, V.; Fan, S.; Levi, O. Sensitivity enhancement in photonic crystal slab biosensors. *Opt. Express* **2010**, *18*, 22702–22714. [[CrossRef](#)] [[PubMed](#)]
18. Wu, F.; Fan, C.; Zhu, K.; Wu, J.; Qi, X.; Sun, Y.; Xiao, S.; Jiang, H.; Chen, H. Tailoring electromagnetic responses in a coupled-grating system with combined modulation of near-field and far-field couplings. *Phys. Rev. B* **2022**, *105*, 245417. [[CrossRef](#)]
19. Bijalwan, A.; Bipin, K.S. Analysis of one-dimensional photonic crystal based sensor for detection of blood plasma and cancer cells. *Optik* **2021**, *226*, 165994. [[CrossRef](#)]
20. Dinodiya, S.; Anami, B. Biosensor Based on One-Dimensional Photonic Crystal for Poliovirus Detection. In *Advancement in Materials, Manufacturing and Energy Engineering*; Springer Nature: Berlin, Germany, 2021; Volume 1.
21. Miyan, H.; Agrahari, R.; Gowre, S.K.; Mahto, M.; Jain, P.K. Computational study of a compact and high sensitive photonic crystal for cancer cells detection. *IEEE Sens. J.* **2022**, *22*, 3298–3305. [[CrossRef](#)]
22. Oskouei, A.; Shojaei, S.S.; Abdollahipour, B. Polarization dependent light propagation in WTe 2 multilayer structure. *Sci. Rep.* **2023**, *13*, 13169. [[CrossRef](#)]
23. Suthar, B.; Anami, B. Enhanced optical sensor for waterborne bacteria-based photonic crystal using graded thickness index. *Appl. Nanosci.* **2023**, *13*, 5399–5406. [[CrossRef](#)]
24. Olyaei, S.; Samira, N. A high-quality factor and wide measurement range biosensor based on photonic crystal nanocavity resonator. *Sens. Lett.* **2013**, *11*, 483–488. [[CrossRef](#)]
25. Efimov, I.M.; Vanyushkin, N.A.; Golik, S.S.; Gevorgyan, A.H. Sensor with enhanced performance based on photonic crystal with a defect layer. *Comput. Opt.* **2023**, *47*, 572–579. [[CrossRef](#)]
26. Efimov, I.M.; Vanyushkin, N.A.; Gevorgyan, A.H. Peculiarities of the Electromagnetic Field Distribution Inside a 1D Photonic Crystal with a Defect Layer. *Bull. Russ. Acad. Sci. Phys.* **2022**, *86* (Suppl. S1), S60–S65. [[CrossRef](#)]
27. Al-Dossari, M.; Awasthi, S.K.; Mohamed, A.M.; Abd El-Gawaad, N.S.; Sabra, W.; Aly, A.H. Bio-alcohol sensor based on one-dimensional photonic crystals for detection of organic materials in wastewater. *Materials* **2022**, *15*, 4012. [[CrossRef](#)] [[PubMed](#)]
28. Edappadikkunnummal, S.; Chembra Vasudevan, R.; Dinesh, S.; Thomas, S.; Desai, N.R.; Kaniyarakkal, S. Detection of Hemoglobin Concentration Based on Defective One-Dimensional Photonic Crystals. *Photonics* **2022**, *9*, 660. [[CrossRef](#)]

29. Hu, J.; Daoxin, D. Cascaded-ring optical sensor with enhanced sensitivity by using suspended Si-nanowires. *IEEE Photonics Technol. Lett.* **2011**, *23*, 842–844.
30. Baraket, Z.; Osswa, S.; Mounir, K. Design of magnetic field direction’s sensor based on a 1D tunable magneto-photonic crystal. *Opt. Quantum Electron.* **2022**, *54*, 637. [[CrossRef](#)]
31. Daher, M.G.; Jaroszewicz, Z.; Zyoud, S.H.; Panda, A.; Hasane Ahammad, S.K.; Abd-Elnaby, M.; Eid, M.M.; Rashed, A.N. Design of a novel detector based on photonic crystal nanostructure for ultra-high performance detection of cells with diabetes. *Opt. Quantum Electron.* **2022**, *54*, 701. [[CrossRef](#)]
32. Almawgani, A.H.; Daher, M.G.; Taya, S.A.; Mashagbeh, M.; Colak, I. Optical detection of fat concentration in milk using MXene-based surface plasmon resonance structure. *Biosensors* **2022**, *12*, 535. [[CrossRef](#)]
33. Yupapin, P.; Trabelsi, Y.; Vigneswaran, D.; Taya, S.A.; Daher, M.G.; Colak, I. Ultra-high-sensitive sensor based on surface plasmon resonance structure having Si and graphene layers for the detection of chikungunya virus. *Plasmonics* **2022**, *17*, 1315–1321. [[CrossRef](#)]
34. Almawgani, A.H.; Daher, M.G.; Taya, S.A.; Colak, I.; Patel, S.K.; Ramahi, O.M. Highly sensitive nano-biosensor based on a binary photonic crystal for cancer cell detection. *Opt. Quantum Electron.* **2022**, *54*, 554. [[CrossRef](#)]
35. Taya, S.A.; Daher, M.G.; Colak, I.; Ramahi, O.M. Highly sensitive nano-sensor based on a binary photonic crystal for the detection of mycobacterium tuberculosis bacteria. *J. Mater. Sci. Mater. Electron.* **2021**, *32*, 28406–28416. [[CrossRef](#)]
36. Panda, A.; Pukhrambam, P.D.; Wu, F.; Belhadj, W. Graphene-based 1D defective photonic crystal biosensor for real-time detection of cancer cells. *Eur. Phys. J. Plus* **2021**, *136*, 809. [[CrossRef](#)]
37. Khani, S.; Hayati, M. Optical biosensors using plasmonic and photonic crystal band-gap structures for the detection of basal cell cancer. *Sci. Rep.* **2022**, *12*, 5246. [[CrossRef](#)] [[PubMed](#)]
38. Winn, J.; Fink, Y.; Fan, S.; Joannopoulos, J.D. Omnidirectional reflection from a one-dimensional photonic crystal. *Opt. Lett.* **1998**, *23*, 1573–1575. [[CrossRef](#)] [[PubMed](#)]
39. Vinogradov, A.; Dorofeenko, A.V.; Erokhin, S.G.; Inoue, M.; Lisyansky, A.A.; Merzlikin, A.M.; Granovsky, A.B. Surface state peculiarities in one-dimensional photonic crystal interfaces. *Phys. Rev. B* **2006**, *74*, 045128. [[CrossRef](#)]
40. Wu, F.; Lu, G.; Guo, Z.; Jiang, H.; Xue, C.; Zheng, M.; Chen, C.; Du, G.; Chen, H. Redshift gaps in one-dimensional photonic crystals containing hyperbolic metamaterials. *Phys. Rev. Appl.* **2018**, *10*, 064022. [[CrossRef](#)]
41. Wu, F.; Liu, T.; Xiao, S. Polarization-sensitive photonic bandgaps in hybrid one-dimensional photonic crystals composed of all-dielectric elliptical metamaterials and isotropic dielectrics. *Appl. Opt.* **2023**, *62*, 706–713. [[CrossRef](#)]
42. Joannopoulos, J.D. *Photonic Crystals: Molding the Flow of Light*; Princeton University Press: Princeton, NJ, USA, 1995; 305p.
43. Yeh, P. *Optical Waves in Layered Media*; Wiley: New York, NY, USA, 1988.
44. Yariv, A.; Yeh, P. *Optical Waves in Crystals*; Wiley: New York, NY, USA, 1984.
45. Vanyushkin, N.A.; Gevorgyan, A.H.; Golik, S.S. Scattering of a plane wave by an inhomogeneous 1D dielectric layer with gradient refractive index. *Opt. Mater.* **2022**, *127*, 112306. [[CrossRef](#)]
46. Fan, X.; White, I.M.; Shopova, S.I.; Zhu, H.; Suter, J.D.; Sun, Y. Sensitive optical biosensors for unlabeled targets: A review. *Anal. Chim. Acta* **2008**, *620*, 8–26. [[CrossRef](#)]
47. Yao, J. Optoelectronic oscillators for high speed and high-resolution optical sensing. *J. Light. Technol.* **2017**, *35*, 3489–3497. [[CrossRef](#)]
48. Qin, J.; Jiang, S.; Wang, Z.; Cheng, X.; Li, B.; Shi, Y.; Tsai, D.P.; Liu, A.Q.; Huang, W.; Zhu, W. Metasurface micro/nano-optical sensors: Principles and applications. *ACS Nano* **2022**, *16*, 11598–11618. [[CrossRef](#)]
49. Van de Velde, F.; Knutsen, S.H.; Usov, A.I.; Rollema, H.S.; Cerezo, A.S. 1H and 13C high resolution NMR spectroscopy of carrageenans: Application in research and industry. *Trends Food Sci. Technol.* **2002**, *13*, 73–92. [[CrossRef](#)]
50. Wang, K.; Vincent, M. High-resolution photoelectron spectroscopy of molecules. *Annu. Rev. Phys. Chem.* **1995**, *46*, 275–304. [[CrossRef](#)]
51. Vanyushkin, N.A.; Gevorgyan, A.H.; Golik, S.S. Approximation of one-dimensional rugate photonic crystals using symmetric ternary photonic crystals. *Optik* **2021**, *242*, 167343. [[CrossRef](#)]

Disclaimer/Publisher’s Note: The statements, opinions and data contained in all publications are solely those of the individual author(s) and contributor(s) and not of MDPI and/or the editor(s). MDPI and/or the editor(s) disclaim responsibility for any injury to people or property resulting from any ideas, methods, instructions or products referred to in the content.